Continental Shelf Research 185 (2019) 3–15

Contents lists available at ScienceDirect

Continental Shelf Research

journal homepage: www.elsevier.com/locate/csr

Benthic controls of resuspension in UK shelf seas: Implications for resuspension frequency

C.E.L. Thompson[a,*], M.E. Williams[b], L. Amoudry[b], T. Hull[c], S. Reynolds[d], A. Panton[d], G.R. Fones[d]

[a] Ocean and Earth Science, University of Southampton, National Oceanography Centre, Southampton SO14 3ZH, United Kingdom
[b] National Oceanography Centre, 6 Brownlow St, Liverpool L3 5DA, UK
[c] Centre for Environment, Fisheries and Aquaculture Science, Pakefield Road, Lowestoft NR33 0HT, UK
[d] School of Earth and Environmental Sciences, University of Portsmouth, Burnaby Road, Portsmouth PO1 3QL, UK

ARTICLE INFO

Keywords:
Celtic Sea
Sediment transport
Resuspension
Shelf Seas Biogeochemistry
Bed stability
Seasonal variability

ABSTRACT

In situ measurements and ship-based resuspension experiments using annular flumes are used to determine sediment stability and critical erosion thresholds for four sites with significantly different sediment characteristics, located in the Celtic Sea at water depths of 100 m. Seasonal and spatial variability of sediment characteristics and erodability is examined, and found to be the result of changes in percentage of organic carbon in the surface sediments (R^2 = 0.82) and bulk density (R^2 = 0.73) respectively when individual characteristic bed parameters are considered. Principal component analysis and linear regression analysis are used to determine a predictive model for erosion threshold in the Celtic Sea (R^2 = 0.99), based on grain size, sorting, kurtosis, bulk density, porosity, percentage fines, organic carbon content and chlorophyll a concentration. Physical sediment characteristics were found to be more significant controls of bed stability than biological factors. Local hydrodynamic conditions are used to determine the likelihood and frequency of resuspension given these critical erosion thresholds. Resuspension is driven by tidal currents, and is common year-round, leading to a constant reworking of bed sediments in particular at the muddier sites. This is confirmed by in situ measurements of suspended sediment concentration.

1. Introduction

The importance of sediment resuspension in shelf seas is well established (Harris, 2014; Nittrouer and Wright, 1994; Solan et al., 2017). In addition to directly influencing the transport of sediment on the shelf (Thompson et al., 2011) and depending on local conditions, resuspension has been shown to: increase or decrease the availability of nutrients and trace metals in the bottom waters (e.g., Couceiro et al., 2013; Katz et al., 2016; Marsay et al., 2014; Parker, 1999); exchange organic carbon with the bed (Morris and Howarth, 1998); limit or induce primary production (Tett and Walne, 1995; Schallenberg and Burns, 2004; Su et al., 2015; Wainright and Hopkinson, 1997); influence oxygen concentrations in bottom waters (Queste et al., 2016) and influence benthic faunal distributions (De Souza et al., 2013). However, the relative importance of these resuspension events on many sediment-water column exchange processes remains unclear; their location, duration and magnitude is difficult to predict; and few in situ investigations of bed stability have been undertaken at typical shelf depths.

One of the key parameters that determine when and where resuspension events take place is the critical erosion threshold (τ_{crit}), which is used to represent the stability (erodability) of the bed. This is often difficult to measure in situ, especially at depth, and often more easily measured bed parameters are used as a proxy for bed stability. Most commonly used is bulk density (e.g., Amos et al., 1997), but a wide range of other characteristic sediment parameters are also used, including (but not limited to) water content (Shi et al., 2015), grain size and roughness (Hong et al., 2015), or the Plasticity index (Jacobs et al., 2011). One of the difficulties with this proxy-based approach is that there are not sufficient or varied enough measurements of bed stability along with the necessary associated sediment properties on the shelf to determine which parameters make the best representative variables. Beyond the physical sediment properties, biological processes also influence sediment stability through biostabilisation (Black et al., 2002), bioturbation (Widdows et al., 2000) or the addition of organic matter; certain faunal behaviours may directly induce resuspension (Cross et al., 2013; Davis, 1993).

The authors began to address the lack of shelf-depth measurements

* Corresponding author.
E-mail addresses: celt1@noc.soton.ac.uk (C.E.L. Thompson), megams@noc.ac.uk (M.E. Williams), laou@noc.ac.uk (L. Amoudry), tom.hull@cefas.co.uk (T. Hull), sarah.reynolds@port.ac.uk (S. Reynolds), anouska.panton@port.ac.uk (A. Panton).

https://doi.org/10.1016/j.csr.2017.12.005
Received 23 May 2017; Received in revised form 7 December 2017; Accepted 9 December 2017
Available online 13 December 2017

of critical erosion threshold with in situ measurements of τ_{crit} using an in situ benthic annular flume in the North Sea (Thompson et al., 2011), although the number of sediment types tested was limited (n = 3), high replication not possible (n = 5), and experiments were only undertaken seasonally at two sites and at two points during the year (April and August 2008): this does not represent the full spatial or seasonal variability of the shelf, which in turn presents difficulties with interpreting the results at a shelf scale. To tackle the problem of replication, recent developments in annular flume design have enabled assessments of critical shear stress of near-undisturbed benthic sediments, collected via box-cores (Thompson et al., 2013), which maintain an intact sediment-water interface. There remains a need however, for more extensive measurements across a continuum of sediment types. Additionally, it is known that sediment stability is highly seasonally dependant in non-shelf environments (e.g., Andersen, 2001; Underwood and Paterson, 1993), as is resuspension in shelf regions (Souza et al., 2007) and important forcing hydrodynamics of the resuspension events themselves (e.g., waves and storms). This paper, based on work carried out under the UK funded Shelf Seas Biogeochemistry Programme presents results collected in the Celtic Sea and expands the existing database of critical threshold measurements on shelf sea sediments. Four new sediment types are investigated, along with an extensive suite of physical and biological bed characteristics, and most importantly revisiting these sites on a seasonal basis structured around a spring bloom event. This allows a more detailed investigation of the controlling variables on sediment stability, which will then allow more accurate predictions of sediment resuspension on the shelf.

2. Methods

2.1. Site description

The Celtic Sea comprises an area of around 70,000 km^2 in the Atlantic Ocean west of the UK, which extends from the shelf-break at ~ 200 m, to a narrow steep coastal zone. Mean spring tidal ranges increase from ~ 3 m near the shelf break to > 12 m in the Severn Estuary (Hydrographic Office, 1996). Although tidal velocities vary across the western shelf region (0.2–1.6 ms^{-1}, Uncles and Stephens, 2007), they tend to be low in the Celtic sea, with bed shear stresses typically < 0.5 Pa in central regions. Winds are Southwesterly or Westerly, and mean wave heights range from 2 m near the shelf break (8 s peak period) to 1 m adjacent to the Irish Sea (6 s peak period) (Bricheno et al., 2015). The water column is well mixed in winter, but weak thermoclines develop in the spring and are associated with the initiation of a spring bloom (Simpson and Sharples, 2012) typically dominated by diatoms (Joint et al., 1986). Bed sediments range from pure muds to gravels (Thompson et al., 2017).

Four discrete sites in the Celtic Sea (Table 1) were selected and visited at seasonal intervals during 2014 and 2015 as part of the Shelf Sea Biogeochemistry (SSB) Programme (Thompson et al., 2017). The four sites (Fig. 1) were chosen as representative of different UK shelf habitats, with significantly different bed sediment types (Table 1) (Thompson et al., 2017). Each site comprised a square of 500 × 500 m in size. Total water column depths were kept constant (94–114 m) to minimise confounding factors between sites. A combination of in situ and on-ship annular flume experiments were used to assess resuspension dynamics at each of these sites, allowing resuspension events to be induced under closely controlled experimental conditions on natural sediment beds. Physical bed characteristics were assessed through core sampling and Sediment Profile Imaging (SPI). Biota was assessed through a combination of coring, trawling and photography. Longer-term monitoring in the form of benthic landers and SmartBuoys were used to assess the short- to medium-term hydrodynamic conditions in the area during the survey period.

2.2. Hydrodynamic monitoring

A series of benthic landers and SmartBuoys were deployed at locations chosen to represent the prevailing hydrodynamic conditions of the four benthic sites (Fig. 1). The East Celtic Deep (ECD), Celtic Deep (CD2L) and Nymph Bank (NB) landers represent sites A and G. East Haig Fras (EHF) represents sites H and I, which are located close to each other. The landers were designed by the Centre for Environment, Fisheries and Aquaculture Science (Cefas) for continuous monitoring of near-bed water column parameters including: conductivity, temperature, pressure, turbidity, oxygen saturation and chlorophyll fluorescence half-hourly for five minute bursts at a sampling frequency of 1 Hz. An upward facing ADCP (RDI 600 kHz workhorse) recorded data hourly in five minute bursts at 1 Hz, providing measurements of currents and backscatter over the bottom ~ 40 m of the water column. Additionally, the National Oceanography Centre (NOC) Liverpool designed miniSTABLE lander was used to provide shorter-term, higher frequency intra-tidal monitoring of: flow velocity, backscatter, acoustic bed morphology/bottom roughness, suspended sediment concentration and size, and nutrients and oxygen. This lander was deployed for approximately 48 h at each site in turn. Cefas designed *SmartBuoys* were positioned close to sites A and G and provided a longer term high-frequency time series (at 1 m below surface) of salinity, temperature, turbidity, oxygen saturation, chlorophyll fluorescence and active light climate. In addition, wave data was provided by an ODAS Buoy located close to the 'Candyfloss' site at 49.4 N, 8.6 W; and the *M5 Wexford Coast wave buoy* (51.69°N 06.704°W), part of the Irish Weather Buoy Network which provides wave parameters to the North of, but closer to, the site locations.

Water column profiles of temperature, salinity, depth, chlorophyll fluorescence and turbidity were also collected, along with water samples for sensor calibration using a Sea-Bird CTD system. Full details of the instrumentation used on the landers and Buoys, as well as deployment locations and durations can be found in Thompson et al. (2017).

2.3. Bed characterisation

Bed sediments were collected using a NIOZ (Haja) Box corer (K16) with 320 mm diameter cylindrical core barrels. Minimal disturbance to the sediment was ensured through careful recovery procedures, and visual rejection of any cores that contained suspended sediment upon retrieval. This provides an 0.08 m^2 core sample with overlying water for use in ship-board resuspension experiments, or for sub-sampling for bed characterisation. Where possible, characterisation sub-cores were taken from within central, undisturbed, sections of the Box cores used in resuspension experiments to minimise any effects of localised small-scale heterogeneity. Grain size was assessed from 10 cm diameter sub-cores (n = 20) using a combination of dry sieving at 0.5 phi resolution (for the fraction > 63 μm) and a LS300 Coulter laser sizer (< 63 μm). Classifications are based on Folk and Ward (1957) geometric graphical (μm) measures, and Folk (1954) textural classes. Bulk density and porosity (n = 12) was assessed using 60 ml syringe sub-cores, extruded and sub sectioned into volumes representatives of known depths between 10 and 30 mm. These samples were dried at 50 °C, and wet and dry bulk densities (ρ_{bw}, ρ_{bd}) calculated. Porosity (φ) was calculated according to Burdige (2006):

$$\rho_{bw} = \varphi\rho_w + (1 - \varphi)\rho_s$$

where ρ_s and ρ_w are the densities of the sediment grains and water respectively.

Organic carbon content (%, n = 3) is approximated using loss-on-ignition (450 °C, 5.5 h, following Grabowski et al., 2011) after drying the samples at 50 °C (Santisteban et al., 2004).

A Sediment Profile Imaging (SPI) camera, manufactured by Ocean Imaging Systems, provided in-situ vertical profile images of the top few centimetres of the seabed, including the sediment-water interface. This

Table 1
Sampling and cruise periods, with central points of each 500 × 500 m process site box and bottom water temperatures.

Site	Benthic A	Benthic I	Benthic H	Benthic G
Central Point Location	51° 12.6754N − 6° 8.0277 E	50° 34.5557N − 7° 6.3161 E	50° 31.3329N 7° 2.142 E	51° 4.3569N − 6° 34.866 E
Sediment Classification	Sandy Mud d_{50} = 57 μm	Muddy Sand d_{50} = 122 μm	Muddy Sand d_{50} = 178 μm	Sand d_{50} = 459 μm
% Fines	> 50%	25–35%	15–25%	< 20%
Cruise[a]	**Start Date**	**End Date**	**Bottom Water Temperature (°C)**	**Description**[b]
DY008 (Pre-Bloom 1)	18 March 2014	13 April 2014	9.38 ± 0.49	Voyager II in situ Flume (A, G, H, I) CMF ship-board Flume (A(4), H(5), I(2))
DY021 (Pre-Bloom 2)	01 March 2015	26 March 2015	9.16 ± 0.05	Voyager II in situ Flume (A, G, H, I) CMF ship-board Flume (A(4), H(4), I(5))
DY030 (Bloom)	04 May 2015	25 May 2015	9.78 ± 0.88	Voyager II in situ Flume (A, G, H, I) CMF ship-board Flume (A(4), H(4), I(4))
DY034 (Late Summer)	06 August 2015	02 Sept 2015	9.69 ± 0.44	CMF ship-board Flume (A(4), H 4), I(4))

[a] Benthic sampling cruises, which took place aboard the RRS Discovery. Cruise reports and data inventories can be found at the following link: http://www.uk-ssb.org/research_cruises/programme.
[b] Number in brackets represent number of replicates for each site.

photographic technique (Rhoads and Cande, 1971; Germano et al., 2011) photographs the sediment-water interface using a Nikon D100 digital camera (F10, 1/60th second, ISO400) and allows assessments of small-scale variations in grain size, sediment colour, surface roughness and biota.

Sediment samples for infaunal analysis were collected using a 500 mm square (0.25 m^2) Scottish Marine Biological Association (SMBA) Box Corer (n = 5). A 2 m Cefas Jennings (Jennings et al., 2012) beam trawl was used for the collection of epifauna from triplicate 5 min trawls carried out a ship speeds of 1.5 knots.

2.4. The resuspension experiments

Two annular flumes were used to measure resuspension at the four sites. Annular flumes are idea for such experiments, as they provide control over the forcing conditions, their channel geometry ensures that applied shear stresses are horizontal in nature, closely replicating natural conditions (Thompson et al., 2013) and their enclosed nature eliminates particles advected from nearby regions (Thompson et al., 2011). Voyager II, a benthic annular flume was used to undertake a series of controlled resuspension events in situ (Thompson et al., 2011). The flume is 2.2 m in diameter and aluminium in construction, with a working channel 0.15 m wide and 0.3 m high. Eight equidistantly

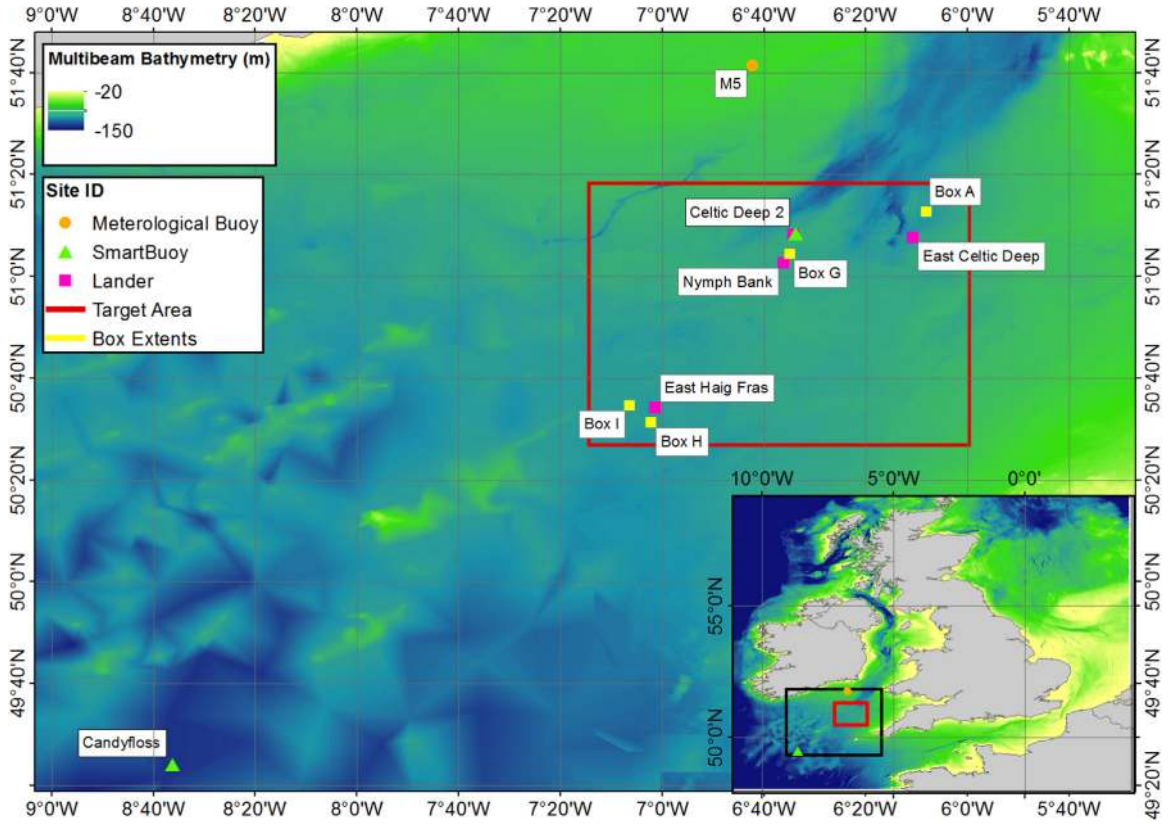

Fig. 1. Site locations, with Lander and Smartbuoy positions within the SSB targeted area (outlined in red). Adapted from Thompson et al. (2017). (For interpretation of the references to color in this figure legend, the reader is referred to the web version of this article.)

Table 2
Bed characteristics. Numbers in brackets represent standard deviations.

	BENTHIC A				BENTHIC I				BENTHIC H				BENTHIC G			
CRUISE	DY008	DY021	DY030	DY034	DY008	DY021	DY030	DY034	DY008	DY021	DY030	DY034	DY008	DY021	DY030	DY034
Water Depth (m)	108.2 (1.2)	109.3 (0.8)	107.2 (0.4)	106.0 (0.5)	109.3 (1.2)	112.2 (0.8)	107.8 (1.5)	109.8 (0.5)	107 (1.1)	109.8 (0.4)	104.3 (0.5)	105.6 (0.4)	98.5 (6.4)	102	99 (1.4)	–
Grain Size (d_{50}, μm)	27.84 (17.18)	46.36 (10.82)	57.84 (17.07)	72.4 (37.2)	96.40 (1.73)	120.58 (37.16)	135.81 (22.85)	101.3 (28.9)	132.12 (34.28)	133.77 (11.38)	260.87 (148.41)	149.1 (45.6)	436.84 (56.03)	519.66 (60.80)	394.94 (182.43)	462.1 (261.3)
Sorting	4.71 (0.38)	4.74 (0.59)	4.91 (0.68)	4.6 (0.4)	5.77 (0.51)	4.57 (0.63)	4.48 (0.97)	4.9 (1.0)	5.05 (1.17)	4.58 (0.67)	3.60 (1.10)	4.3 (1.6)	2.78 (1.35)	2.08 (0.24)	2.81 (1.49)	4.3 (2.9)
Skewness	− 0.27 (0.28)	− 0.39 (0.05)	− 0.48 (0.06)	− 0.5 (0.1)	− 0.45 (0.06)	− 0.41 (0.07)	− 0.37 (0.11)	− 0.5 (0.1)	− 0.36 (0.07)	− 0.4 (0.05)	− 0.39 (0.08)	− 0.3 (0.2)	0.24 (0.16)	− 0.24 (0.12)	− 0.33 (0.17)	− 0.5 (0.1)
Kurtosis	0.82 (0.21)	0.92 (0.04)	1.01 (0.06)	1.1 (0.2)	1.14 (0.21)	1.36 (0.20)	1.43 (0.13)	1.3 (0.3)	1.19 (0.52)	1.35 (0.22)	1.45 (0.25)	1.4 (0.3)	1.68 (1.7)	2.04 (0.69)	2.03 (0.71)	2.3 (1.1)
% Mud	68.70 (5.93)	58.08 (6.22)	52.55 (9.34)	47.8 (13.0)	33.09 (1.19)	28.41 (5.86)	24.58 (5.40)	34.1 (10.8)	25.84 (7.91)	25.67 (3.75)	17.32 (9.65)	22.4 (11.9)	3.38 (1.99)	5.26 (1.28)	15.07 (20.46)	21.5 (21.1)
Dry Bulk Density ($kg\,m^{-3}$)	620(30.86)	516.97 (145.71)	692.73 (92.48)	863.22 (124.18)	1091.82 (55.28)	986.67 (211.22)	1064.85 (312.05)	865.45 (56.01)	1100.18 (14.14)	1199.39 (234.12)	1000.61 (198.44)	1150.91 (211.82)	1290(345.84)	1471.52 (112.88)	1520(95.88)	1748.48 (80.00)
Porosity (%)	0.62	0.70	0.72	0.69	0.54	0.66	0.55	0.62	0.48	0.55	0.48	0.53	0.44	0.38	0.39	0.58
Permeability ($\times 10^{-15}$)	5.92	12.86	15.07	52.48	91.24	110.91	232.65	182.79	290.09	256.16	1254.00	494.15	8574.01	8330.91	4917.28	5922.50
Chlorophyll a ($\mu g\,m^{-2}$)	1.66	0.68	2.10	1.28	0.52	0.60	0.22	0.54	0.30	0.64	0.48	0.24	0.49	0.08	0.14	0.62
Organic Carbon (g^{-2})	1.02	1.23	1.34	1.16	0.48	0.56	0.68	0.60	0.31	0.46	0.36	0.40	0.11	0.12	0.15	0.49
Infaunal (macro) Carbon (g^{-2})	20.80 (41.12)	7.66 (11.26)	37.71 (114.47)	7.80 (12.84)	13.64 (30.33)	1.93 (2.39)	3.58 DY(4.48)	4.09 (4.56)	9.23 (10.81)	3.87 (4.43)	13.90 (16.78)	13.26 (16.64)	6.02 (5.71)	8.94 (24.03)	16.82 (27.35)	9.97 (14.71)
Epifaunal Carbon (g^{-2})	–	10.02 (2.30)	2.88 (1.39)	10.00 (7.94)	–	2.46 (0.35)	2.78 (1.21)	2.22 (0.78)	–	2.23 (1.45)	1.65 (0.71)	1.75 (1.32)	–	6.45 (1.59)	9.57 (0.89)	3.34 (1.93)
Oxygen Penetration Depth (cm)	1.6	0.8	0.3	0.8	1.5	0.2	0.3	0.9	1.5	0.9	0.8	0.3	1.4	5	1.4	0.5
Bioturbation Potential	12.2 (4.28)	0 (0)	1.91 (2.85)	2.37 (0.67)	5.38 (2.76)	4.96 (3.29)	1.88 (2.60)	4.50 (2.84)	13.85 (3.45)	5.93 (3.14)	5.25 (2.48)	9.44 (1.46)	6.81 (4.87)	1.45 (1.37)	5.48 (2.81)	2.81 (1.58)

spaced paddles induce a current and are driven by a programmable 24 V DC motor and gearbox, using a chain drive. Flow velocities are recorded using a Nortek Vectrino Velocimeter (ADV) measuring along (u), across (v) and vertically (w) within the channel, at a height of 0.15 m above the nominal bed level. Suspended particulate matter concentrations (SPM) are assessed using three optical backscatter sensors (Seapoint OBS) measuring turbidity at three heights within the channel, calibrated using gravimetric analysis against water samples taken using an automated 12 × 50 ml syringe sampling system, and converted to inorganic suspended sediment concentration (S) using loss-on-ignition. The flume was pre-programmed with lid rotational speeds and water sampling times, and data recorded onto an onboard logger. The flume was lowered to the seabed, and the ship kept on position using dynamic positioning for the duration of the experiments (~ 2 h). Cable-mounted buoys positioned approximately 10 m above the flume were additionally used to ensure it was isolated from any surface boat motions.

Due to the length of time required to deploy the Voyager II flume and the cruise schedules, replicate in situ deployments were not possible. Therefore, the ship-board Core Mini Flume (CMF, Thompson et al., 2013) was used for replicate resuspension experiments to determine the effects of small-scale spatial heterogeneity within sites A, I and H. The CMF is a small annular flume of acrylic construction, 0.2 m in diameter, with a working channel 0.04 m wide and 0.3 m in height. Four equidistant paddles are used to drive the flow, controlled by a digital stepping motor. Velocities were measured using a Nortek Vectrino 'side looking' ADV where space allowed, or against calibrations based on lid-rotation if not ($R^2 = 0.80$, $p < 0.01$). Three D&A Instruments OBS allowed the measurement of SPM, which was calibrated against water samples taken manually by syringe at regular intervals throughout the experiments. The flume was designed to fit within a standard 0.3 m (or larger) circular box core barrel, which were collected using the NIOZ (Haja) corer. This allowed the collection of several intact sediment cores with overlying bottom water, which were stored in a temperature controlled container set at bottom temperature for the duration of the resuspension experiments. The sediment cores for the sandy site G could not retain sufficient head of water for the duration of the experiments, and so resuspension is only measured in situ.

In both cases, applied shear stress at the bed was increased in a stepwise fashion, through incremental increases in paddle speed following Thompson et al. (2011, 2013). Each step lasted for either 10 (in situ; high resolution ship-board) or 20 (ship-board) minutes and were designed to identify the critical erosion threshold of the bed. Calibrated OBS data were used to calculate time series of SPM and S (inorganic suspended sediment concentration), which was averaged over 20 s to eliminate high frequency, short-term variability (Widdows et al., 2007) and normalised to starting concentration for inter-comparability. Shear stresses were adjusted for stress reduction induced by increasing sediment concentrations over the duration of the experiment, following Amos et al. (1992), Amos et al. (2003) and Li and Gust (2000):

$$u_{*s} = u_* - \left(0.2267[\log_{10}S]\frac{u_*}{6.35}\right), \text{cm. s} - 1$$

Erosion rate (E, kg m^{-2} s^{-1}) was calculated following:

$$E = \frac{\delta M}{\delta t} = \frac{[V(S_{end} - S_{start})]}{\Delta t A}$$

and equivalent depth of erosion from:

$$\frac{dz_e}{dt} = \frac{dM}{dt}\frac{1}{A\rho_b}$$

where M is the eroded dry mass of sediment (kg), V is the flume volume (m^3), A is flume bed area (m^2) and Δt is the duration (s) of the applied shear stress.

The critical erosion threshold is interpreted as the point of initial erosion of the bed, and was determined through a linear regression of the time-averaged SPM measurements to (log) applied bed shear stress (Pa) related to ambient conditions in the flume, following the method of Thompson et al. (2011), Sutherland et al. (1998), Amos et al. (2003) and Widdows et al. (2007), which discuss the complexities of the methodology, and it's limitations in detail. The method has been found to be accurate even in cohesive sediments with high proportions of fine sands (Sutherland et al., 1998).

3. Results

3.1. Sediment characteristics

The full bed characteristics for the four sites are summarised in Table 2, split across the four cruises. Given values are means (typically averaged over 3–4 replicate cores), with standard deviations in brackets. As would be expected, there is considerable variability between sites, but there is also evidence of within site variability, both seasonally (between subsequent cruises) and spatially (as seen in the standard deviation values of replicate cores, and statistically assessed using the Central Limit Theorem).

3.1.1. Spatial variability

Benthic A is the muddiest of the four sites, made up of over 50% fine sediment (< 65 μm) overall, which is reflected in low bulk density and permeability measurements. It exhibits the highest concentrations of surface chlorophyll *a* and organic carbon, as well as the highest infaunal and epifaunal biomass of all the sites visited. Benthic G, is the sandiest site (< 20% fines), with the highest bulk density and permeability. It exhibited the lowest organic carbon content overall, the lowest chlorophyll *a* concentrations during the pre- and bloom phases of the programme and faunal carbon contents in the mid-range of all the sites.

Benthic I and H are both muddy sands, although benthic I (fines ~ 30%) has a lower bulk density and permeability than H (fines ~ 20%). Chlorophyll *a* concentrations were comparable in magnitude between the two sites, although some differences can be seen in seasonal signals. Organic carbon content and epifaunal content were highest at benthic I, but infaunal carbon was generally highest at H.

In all cases, standard deviations illustrate intra- and inter- site variability, used to determine whether the sites are significantly different in terms of sediment characteristics. This was the case in general ($p < 0.05$), with the following exceptions. H and G show increased local heterogeneity in grain size during the spring bloom. Benthic I and H aren't significantly different in terms of % fines for either the pre- or bloom cruises, nor are I and G for bloom and late-summer conditions. Bulk density was highly locally variable during the Pre Bloom (1) cruise.

3.1.2. Seasonal variations

At Benthic A, an increase in median grain size of ~ 45 μm is observed throughout the year, although there is little change in the other size distribution parameters (sorting/skewness etc.), and given the within site variability, this is only significant between the first two pre-bloom cruises ($p < 0.05$). The percentage of fines decreased alongside this change in grain size (significant between the two pre-bloom cruises), with bulk density increasing significantly between pre-bloom and bloom conditions, and between the bloom and late-summer cruises ($p < 0.05$). Chlorophyll *a* peaked during the spring bloom and this is reflected in the amount of organic carbon in the surface sediment layers. Infaunal carbon also peaks during the bloom, although epifaunal carbon was at a minima.

For Benthic I, the grain size is largest during the bloom, and drops again in the following cruise (total range ~ 40 μm; differences significant to $p < 0.05$). The percentage of fines also shows a minima at the same time, although not to a significant degree, and this is reflected

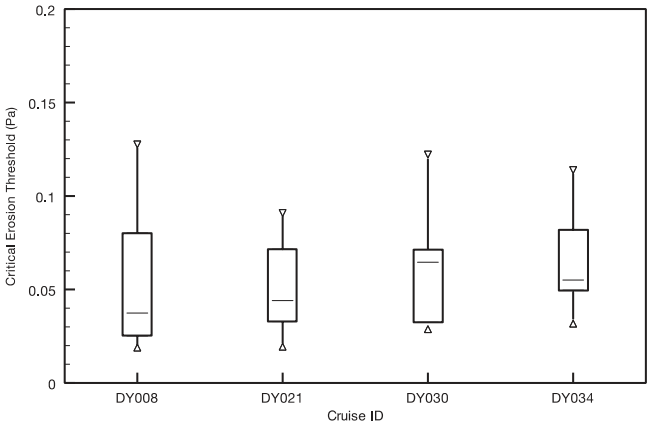

Fig. 2. Box and whisker plots of critical Shear stresses for all in situ and ship-board experiments.

in a maximum bulk density value (significant between bloom and late-summer; $p < 0.0001$). Chlorophyll *a* is actually at a minima during the bloom, although the amount of organic carbon found in the surface sediments, and the amount of epifaunal carbon both peak during this time. Infaunal carbon increases between pre bloom to late-summer cruises.

For Benthic H, the grain size is also largest during the bloom, but falls within the variability of the site (total range ~ 130 μm); however the bulk density increases significantly throughout the year to peak late-summer ($p < 0.05$). Chlorophyll *a* is greatest in late-summer, as is organic carbon. Both infaunal and epifaunal biomasses are highest during the bloom.

For Benthic G, the grain size peaks pre-bloom (2), although subsequent differences are within the site variability (total range ~ 125 μm). Percentage of fines is greatest in late-summer, although high within site variability here masks any significant seasonal signal. However, changes in bulk density are significant seasonally, increasing throughout the year to peak in late-summer ($p < 0.001$).

3.2. Resuspension dynamics

Fig. 2 illustrates the ranges of measured critical shear stresses based on month of collection. Table 3 summarises the key results of the resuspension experiments, including the critical erosion thresholds, peak erosion rates and equivalent depth of erosion.

3.2.1. Spatial variability

The significance of any differences in critical erosion threshold are assessed against within-site variability from replicate ship-board experiments with the core miniflume, using the central limit theorem. Overall, a consistent pattern is observed regarding the strength of the sediment, with A having the lowest critical erosion threshold, followed by I, H and finally G having the highest. There appears to be no significant ($p < 0.05$) differences in critical erosion threshold between Benthic A, I and H for the first pre-bloom cruise. During the second pre-bloom cruise, there are significant differences in critical erosion threshold between A and H, as well as between A and I, with A being easier to erode in both cases; but not between H and I themselves. This changes during the bloom, where there are significant ($p = < 0.01$) differences between all three sites with the lowest values found for A and the highest for H; these differences are also seen during the late-summer cruise ($p < 0.05$). In situ measurements show greater variability during the initial pre-bloom cruise, with Benthic H being the most stable, followed by I, G and finally A. However, without replication, it is not possible to determine whether these are statistically significant differences. The in situ results are generally higher during this initial cruise than those measured using the CMF. For the subsequent pre-

Table 3
Resuspension characteristics. Values in brackets are standard deviations for averages of replicate experiments.

	FLUME	SITE A				SITE I				SITE H				SITE G			
		DY008	DY021	DY030	DY034	DY008	DY021	DY030	DY034	DY008	DY021	DY030	DY034	DY008	DY021	DY030	DY034
Critical Erosion Threshold (Pa)	Voyager	0.068 – (R^2 = 0.85)	0.020 (R^2 = 0.87)	0.041 (R^2 = 0.73)	–	0.103 (R^2 = 0.79)	0.044 (R^2 = 0.88)	0.065 (R^2 = 0.61)	–	0.128 (R^2 = 0.84)	0.053 (R^2 = 0.73)	–	–	0.085 (R^2 = 0.78)	0.072 (R^2 = 0.6)	0.203 (R^2 = 0.72)	–
	CMF	0.027 (0.0016)	0.030 (0.0079)	0.031 (0.0015)	0.044 (0.011)	0.029 (0.012)	0.056 (0.016)	0.058 (0.017)	0.056 (0.011)	0.037 (0.033)	0.064 (0.030)	0.096 (0.034)	0.093 (0.016)	–	–	–	–
Peak Erosion Rate ($kg\,m^{-1}\,s^{-1}$)	Voyager	0.0037 (0.013)	0.00129 (0.028)	0.00222 (0.0017)	– 0.0017 (0.0016)	0.0127 0.011 (0.0064)	0.00150 0.028 (0.026)	0.00283 0.0094 (0.0064)	– 0.017 (0.032)	0.0127 0.044 (0.035)	0.0158 0.038 (0.047)	– 0.012 (0.011)	– 0.019 (0.022)	0.00150 –	0.00276 –	0.00144 –	– –
	CMF	0.011 (0.013)	0.019 (0.028)	0.0037 (0.0017)													
Equivalent Depth of Erosion (mm)	Voyager	0.79	0.103	0.106	–	0.417	0.07	0.05	–	0.325	0.078	–	–	0.044	0.017	0.057	–
	CMF	8.24 (10.51)	9.19 (9.95)	4.42 (4.69)	0.695 (0.382)	5.94 (5.388)	6.59 (6.673)	3.11 (3.272)	1.35 (1.98)	10.04 (8.126)	23.53 (23.06)	6.34 (6.82)	3.93 (1.249)	–	–	–	–

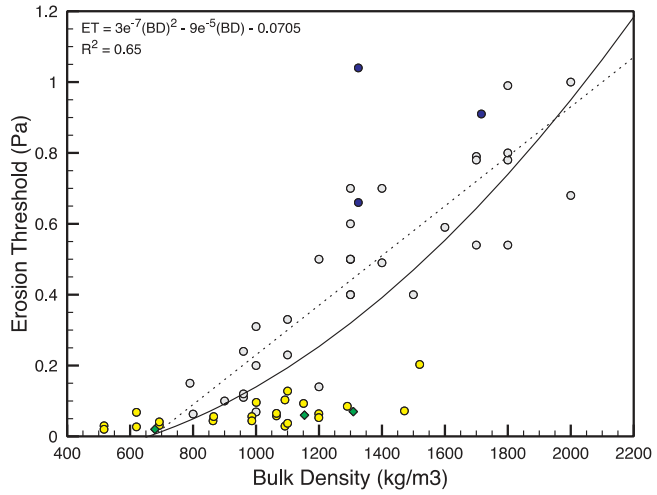

Fig. 3. Erosion threshold vs. Bulk density, overlaid on coastal field data collected using the in situ Sea Carousel from Amos et al. (1997) (grey, with regression as dotted line). Celtic Sea (yellow), North Sea (Thompson et al., 2011; blue); UK Coastal (Thompson et al., 2013; green diamonds), regression for all data as solid black line and equation. (For interpretation of the references to color in this figure legend, the reader is referred to the web version of this article.)

bloom (2) cruise, bed stability is least at A, intermediate at I and H, and peaks for G. This pattern continues into the spring bloom, and agrees with the findings of the CMF experiments, with similar magnitudes.

3.2.2. Seasonal variability

Significant seasonal variability was seen as an increase in critical erosion threshold between the bloom and late-summer periods at Benthic A, and between the pre-bloom and bloom conditions for Benthic H and G. There were no apparent seasonal trends for Benthic I. Differences between the two pre-bloom cruises were noted, and may be the result of extreme wave conditions experienced around the UK in the winter period of 2013/14 (Masselink et al., 2015), which were a- typical of the region

Depths of erosion for the experiments did not exceed 2.5 cm into the bed, although in several cases (A and I in pre-bloom (2) and bloom conditions; H in late-summer conditions) it exceeded (by up to 0.4 cm (see Tables 2 and 3)) or matched measured oxygen penetration depths. Peak erosion rates typically followed the same variation pattern as the critical erosion thresholds.

4. Discussion

Note that a series of large storms occurred shortly before the initial pre-bloom (1) cruise in 2014 (Masselink et al., 2015), which may have resulted in a greater remobilisation of the bed than normal and removal of the surface layers of sediment. Because it is difficult to determine whether this year is typically representative of the UK shelf, and there is only a single time point for March of that year it will be omitted from the discussion unless specified.

Measurements of bed stability are useful for informing site-specific resuspension and exchange dynamics. This is particularly true of the Celtic Sea, where existing literature on resuspension is focussed on the shelf edge and continental margin regions (Thomsen and Gust, 2000; Thomsen and McCave, 2000). Additionally, in order to assess exchange across the sediment-water interface at a shelf scale these measurements must be scaled-up, and the likelihood of resuspension events occurring must be predicted. The first steps towards doing this, which are undertaken in the presented work, are to: (1) be able to predict the critical erosion threshold and therefore the stability of the bed given commonly measured bed characteristic data; and (2) to assess the likelihood that local hydrodynamic conditions will exceed the critical erosion threshold.

4.1. Predicting variability in critical erosion threshold from bed characteristics

Due to the lack of available data and the difficulty in measuring critical erosion thresholds in situ (Thompson et al., 2011, 2013), it is common to predict bed stability from individual-parameter predictors (e.g., Amos et al., 2003; Hong et al., 2015; Jacobs et al., 2011; Shi et al., 2015). When sediment characteristics (Table 2) are considered individually for the Celtic Sea, the seasonal trends described above (Table 3) are closely related to the amount of organic carbon in the near-surface sediments (R2 = 0.82). Such a clear relationship was not observed in similar experiments undertaken in the North Sea (Thompson et al., 2011), where limited temporal experiments were carried out, but it is in general agreement with laboratory (Young and Southard, 1978) and in situ measurements in shallow water environments (Andersen, 2001; Amos et al., 2010) and emphasises the need for a seasonal experimental design to be used in investigations of shelf sediment stability. Spatial variability between sites was most closely correlated to the physical characteristics of the sediments (Table 2), including the bulk density (R^2 = 0.73); grain size (R^2 = 0.68); and porosity (R^2 = 0.76). Given the within-site (between-replicate) variability of some of these parameters however, the bulk density appears to be the most robust of these predictors, and the general trend agrees with other relationships derived using annular flumes in shallow coastal sites (Amos et al., 1997; Fig. 3) showing an increase in stability with increasing bulk density. The Celtic Sea sediments exhibited a wide range of bulk densities (Table 2), given the narrow water column depth range of the sites visited. At lower bulk densities, the erosion thresholds fit well with the existing relationship to stability based on coastal measurements; however, these tend to over predict at higher bulk densities. This may be an effect of water column depth differences between the shelf and coastal settings. A relationship combining all available data (Fig. 3: ET = $3e^{-7}(BD)^2 - 9e^{-5}(BD) - 0.0705$; R^2 = 0.65, where ET = erosion threshold; BD = bulk density), explains 65% of the variance in erosion threshold, but is non-linear, suggesting that site-specific, or depth-dependant relationships may be more appropriate, reflecting the complex and often co-varying nature of many sediment characteristics.

It is clear that the overall variability in sediment characteristics and stability seen between the sites and over the entire study period is complex, and is likely being controlled by a combination of physical and biological characteristics of the sites. As such, a multi-parameter model may be more likely to accurately predict critical erosion thresholds at the shelf scale. Principal component analysis was therefore carried out using all the bed characteristic data available (Table 4), which indicates that 85% of the variance in the bed samples can be explained by 3 components. The first (PC1) is comprised mainly of physical bed characteristics (most importantly median grain size, sorting, kurtosis and porosity), with the second and third containing biological factors (chlorophyll *a*, epifauna and infauna), indicating the relative importance of the physical bed characteristics, and informing the choice of parameters for multiple-linear regression analysis.

A multiple linear, least-squares fit, regression analysis was carried out to determine the strongest controls specifically for the critical shear stress for resuspension (Table 4), to form the basis of a predictive model. This confirms the strong relationship between those parameters indicated in PC1 and critical erosion thresholds, but does not show strong dependence on the parameters contained in PC2 or PC3.

This suggests that the bed becomes more stable with increasing grain size as predicted by standard sediment threshold curves (see review in Paphitis, 2001), but also with better sorting and more specifically with higher lepturkuticity (better sorting in the central portion of the samples than in the tails). Such sorting related effects are typical of sand and soil transport (Komar, 1987; Pye and Tsoar, 2009) where

Table 4
(a) Principal component analysis (PCA) of bed characteristics. Blank space indicates a regression coefficient < 0.3. Values in bold indicate key parameters (R > 0.8). (b) Multiple linear regression against critical shear stress for erosion, giving Pearson's correlation coefficients. Bold values indicate significant relationships (2-tailed, p < 0.05).

	(a)			(b)
	PC1	PC2	PC3	MLR; t_{crit}
Median Grain Size	**0.964**			**0.680**
Sorting	**− 0.908**			**− 0.664**
Skewness	0.516	− 0.573		0.462
Kurtosis	**0.896**			**0.772**
% Fines	**− 0.800**	0.394	0.415	**− 0.639**
Bulk Density	**0.843**		− 0.364	**0.733**
Porosity	**− 0.860**	0.386		**− 0.766**
Chl A	− 0.434	**0.867**		− 0.469
Benthic Carbon	− 0.744	0.504	0.412	**− 0.677**
Oxygen Penetration Depth	0.706		0.503	0.201
Epifauna			**0.855**	0.093
Infauna		**0.892**		0.028
Bioturbation Potential			− 0.775	0.490
% Variance	56.9	16.5	11.5	

packing and exposure effects in poorly sorted sediments can lead to earlier than predicted movement of the bed, but for which there is little research in cohesive marine sediments. It should be noted, however, that changes in grain size are often associated with changes in sorting and so these factors are likely co-varying.

Increases in the percentage of fines appear to reduce bed stability. Fines in this context include any material with a physical size smaller than 65 μm. As such, this relationship may indicate that the sediments do not have a sufficient clay content to act cohesively (Ahmad et al., 2011), even though they are comprised of fine material. Typically quoted as mud concentrations ranging from 3% to 15% according to Mitchener and Torfs (1996), up to 20–30% as found by Houwing (2000), cohesiveness depends heavily on the clay mineralogy and content of that fines component (Van Ledden, 2003). Alternatively, it may imply that the grain size ratio (the relative size of the coarse and fine fractions of the sediment) of these mixed sediments is low (Staudt et al., 2017), which may result in preferential winnowing and sorting under applied stresses (Low et al., 2008). However, it may simply be related to the corresponding decreases in bulk density and consolidation that are also associated with increased fines percentages across these sites. Increasing bulk density (and the closely related porosity) indicates higher bed strength. Finally, increasing organic carbon in the surface sediments decreases bed stability, potentially a result of the lower density of organic material (Morris et al., 2016) lowering the overall bulk density of the sediment, but more likely as a result of differential winnowing (Low et al., 2008) as with fines percentage, again highlighting the co-varying nature of many of the sediment properties.

Similar relationships have been observed in the North Sea (Thompson et al., 2011), with two principal components explaining the variance: PC1 comprising mainly physical parameters and PC2 biological ones. There were some key differences in the multiple regression analysis, which indicate a negative relationship between grain size and critical shear strength, a stronger relationship with skewness, and weaker relationships with % fines and bulk density. However, it should be noted that n = 5 for the North Sea, whereas the current work has n = 24, and is therefore more robust.

A simple predictive model for estimating critical shear stresses based on commonly measured bed characteristics was constructed (units defined in Tables 2 and 3). The results of the PCA and multiple linear regression analysis were used to focus this model initially, and stepwise regression used to fine tune for the best possible fit given all the available data. It should be noted that epifaunal carbon data was not available for the initial pre-bloom (1) cruise undertaken in March 2014, and, given the unusual storm conditions experienced during that year these data are not considered in the model results.

The best model fit (R^2 = 0.98) for the Celtic Sea data was one which, as suggested by the PCA, principally includes the physical characteristics of the sediment, but in which optimisation of the model suggests inclusion of chlorophyll *a* (one of the key parameters in PC2). However, neither epifauna nor infaunal variation appear to have a significant control over bed stability.

Model 1:

$$\tau_c = 0.0209d_{50} - 0.1975\sigma + 0.473K + 0.00359\%Fines - 0.0002025\rho_B - 0.676n + 0.080984ChlA - 0.17862\%C + 1.1571.$$

Adjusted R^2 = 0.98, p < 0.001, RMS error = 0.027.

where σ = sorting, K = kurtosis, ρ_B = bulk density, ChlA = chlorophyll a, n = porosity and %C = percent carbon.

When this relationship was applied to the data from the North Sea, a reasonable fit was found (R^2 = 0.47), but the model over-predicted the bed strength. A better fit here (R^2 = 1; RMS error = 0.3) was found using physical parameters alone:

Model 2:

$$\tau_c = 0.0301456d_{50} + 0.64646\sigma + 1.5355K + 0.10278\%Fines - 0.007098\rho_B.$$

This may be due to the higher and less variable chlorophyll *a* concentrations found at these sites, due to their shallower depths (30–80 m); less of a seasonal signal in chlorophyll *a* was evident for the North Sea as these experiments were undertaken either side of the spring bloom, but not during it. Applying this second model to the Celtic Sea data resulted in a very poor fit, over predicting bed strength considerably, as did applying the model to a data set consisting of very shallow locations (14–130 m, Thompson et al., 2013, n = 4) which lacked any corresponding biological data.

A model incorporating data from both shelf-seas could be constructed, which predicts either sets of data (adjusted R^2 values = 0.98, p < 0.001, RMS error = 0.054), however its over-complicated nature (including 15 separate parameters) precludes its usefulness.

It is clear that the complexity and variability of shelf-sea sediments in general, and the controls of sediment stability specifically, do not necessarily lend themselves to a simple single-parameter predictor of resuspension in these regions. Spatial variations may be predicted based on relatively simple models of easily measured physical parameters (e.g., Model 2), however, when seasonal and biological factors are considered, the large differences in benthic assemblages (Widdows et al., 2007), and biological processes, in geographically distinct shelf-sea regions results in overly complex predictors that require a large amount of data to be collected. In addition to this, the potential feedbacks between changes in bed composition due to resuspension and the resulting benthos must be considered. It is recommended therefore, that predictions of bed stability for the purposes of scaling up to shelf-scales, are based on the collection and assessment of moderate amounts of localised data (including particle size distributions, bulk density, Chlorophyll a and percent carbon as used in Model) specific to the shelf region being investigated, rather than trying to establish a general 'Shelf-sea' model, and that while single parameter models are less robust predictors of bed stability in shelf seas, if a single parameter model is to be used, that bulk density is both easily measured and exhibits significant relationships both spatially and seasonally. Further consideration must also be made concerning the hydrodynamic setting and its effect on threshold of erosion. Depth variations, and associated differences in bed consolidation times or hydrodynamic forcing may have a lasting effect on the bed sediments in terms of a stress-history, which is not captured in predictors based solely on the physical or biological characteristics of the bed.

4.2. Likelihood of resuspension

Two sets of data are available to allow us to assess the likelihood and frequency of resuspension events in the Celtic Sea: short-term, high resolution miniSTABLE lander data (co-located with the main sampling sites, but only available at all sites for the late-summer period in August 2015); and long-term Cefas lander data (not directly co-located with the resuspension experiment locations).

4.2.1. Short-term, high resolution shear stress measurements

Applied bed shear stresses (τ) were calculated based on ADV data collected 0.3–0.65 m above the bed (depending on deployment) and calculated using the Law of the Wall:

$$u_z = \frac{u_*}{\kappa} ln \frac{z}{z_0}$$

$$\tau = \rho U_*^2$$

where u_z is the measured horizontal velocity, at a height of z above the bed, u_* is shear velocity, κ is the von Karmen constant (0.41), and z_0 is the roughness length. The calculation of bed stress is highly dependant on z_0. The possible range of bed stresses is thus predicted by the grain size dependant $z_0 = d_{50}/12$ which assumes a flat bed (red lines in Fig. 4) to an estimate using the largest bedform dimensions (using a ripple relationship: $z_0 = 6$ mm; Soulsby, 1983) as observed in sonar bedscans of the site (Thompson et al., 2017).

Fig. 4 shows the ranges of applied shear stresses measured at each of the sites during the late-summer deployments in August 2015, overlaid with the critical shear stresses measured during the cruise. Clear quarter and semi-diurnal variations associated with the tide are evident, but it should be noted, that lander deployments were not at the same stage of the spring-neap tidal cycle for each site, and are therefore not directly comparable. At Benthic A, the muddiest site, applied shear stresses are always in excess of the minimum critical shear stresses, which are close in magnitude to the lowest applied stresses predicted at the site. This implies frequent resuspension and re-working of the bed sediment. Benthic I, with ~ 30% fines, shows a higher resistance to resuspension, with applied stresses exceeding criticals during higher magnitude events (based on lower limits of z_0) or during the peak flows of each tidal cycle (higher limit of z_0). At Benthic H (~ 20% fines), resuspension also occurs during peak velocities (high z_0). For Benthic G (< 20% fines), the applied shear stresses rarely exceed the critical shear stress during the measurement period. The deployments at Benthic G and I both take place during neap tides, while deployments at A and H take place during spring tide, and 3 days after maximum spring tide respectively. This implies that the frequent resuspension seen at A may indicate an upper limit, and may over-estimate total resuspension events over the complete spring-neap cycle. Resuspension at G and I has the potential to be higher than predicted. An examination of longer-

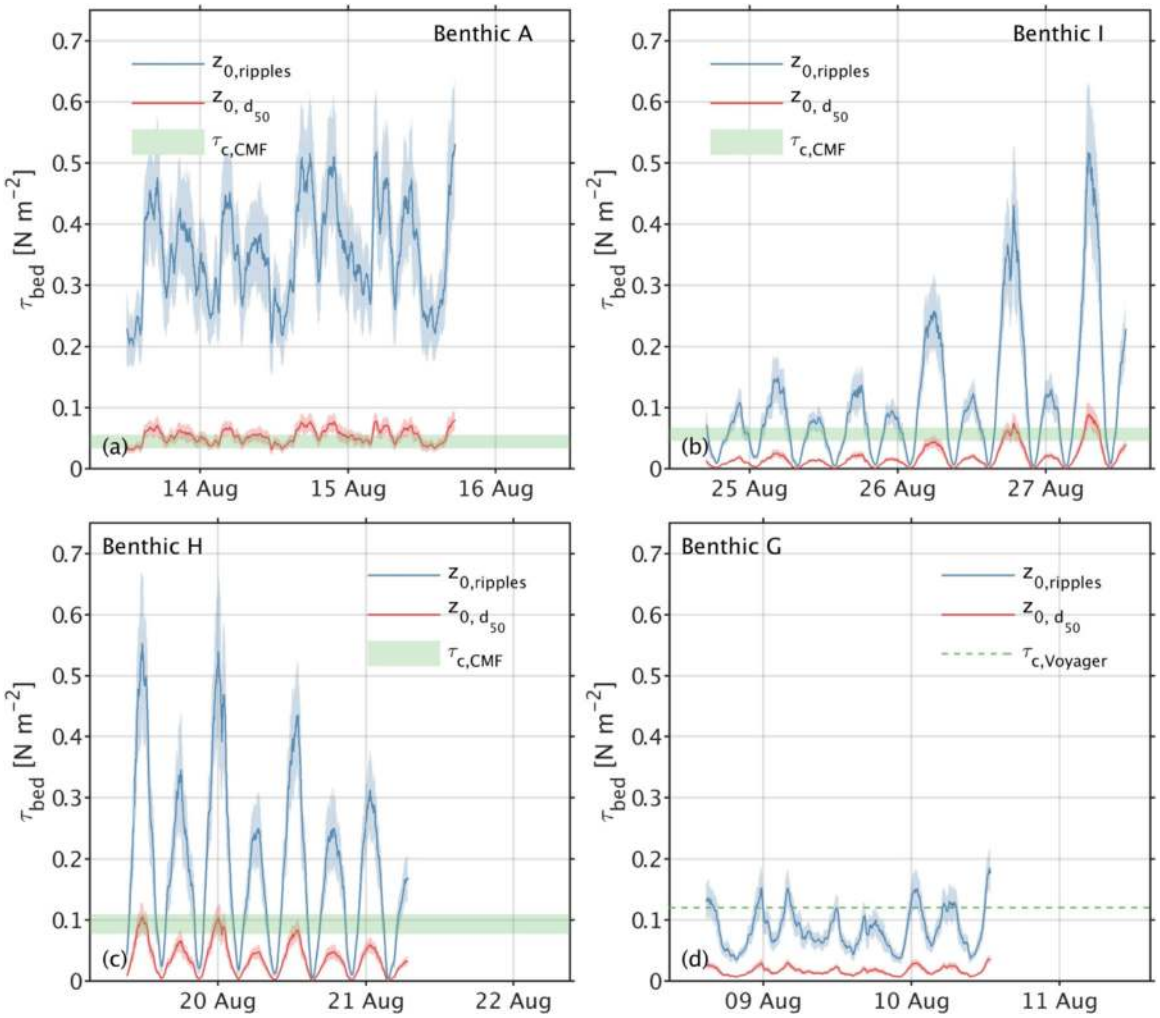

Fig. 4. Mean applied shear stresses (shading representing standard deviation) for the upper (blue) and lower (red) z_0 limits overlaid with critical shear stress ranges (green shading) representing CMF data using sediment collected during the miniSTABLE lander deployment period (Over spring tides for Benthic A and H; neap for G and I)). For Benthic G the dashed green line represents the average critical shear stress measured over all cruises. (For interpretation of the references to color in this figure legend, the reader is referred to the web version of this article.)

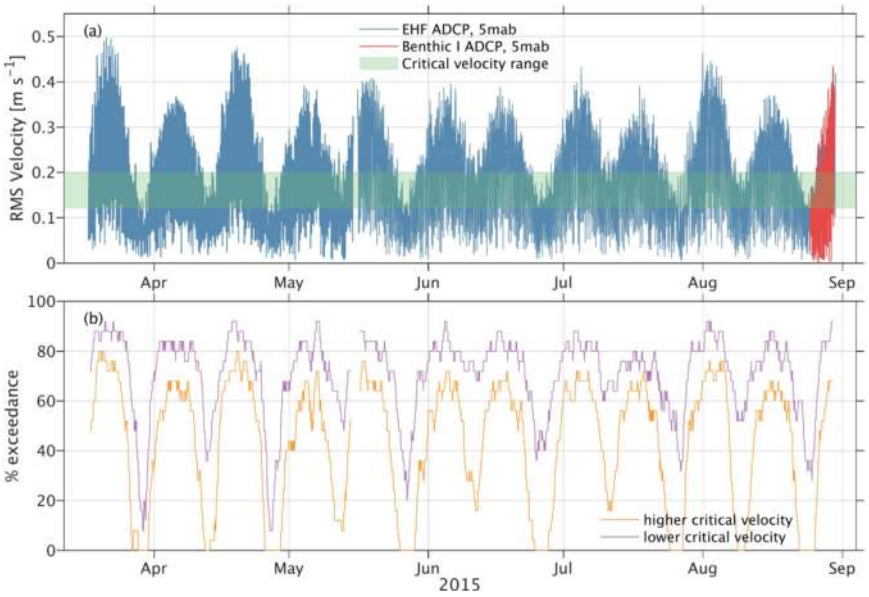

Fig. 5. Top: Flow velocity 5 m above the bed (a) as measured by the long term Lander East of Haigh Fras ADCP (blue), overlaid with same measured from the Benthic I miniSTABLE lander ADV, and critical velocities measured at Benthic I (green). Exceedance of critical velocities (b) based on a 25 h moving window. (For interpretation of the references to color in this figure legend, the reader is referred to the web version of this article.)

term measurements is needed to fully assess likelihood of resuspension, however, this short-term data series indicates that the resuspension potential is highest at Benthic A, and lowest at Benthic G, and is correlated with percentage fines.

4.2.2. Long-term shear stress measurements

Fig. 5 shows the applied and critical velocities measured over several months during the study period for Benthic I and the East of Haig Fras lander. Critical velocities at 5 m above the bed were derived from the critical shear stresses measured using the miniSTABLE ADV data, to address a lack of confidence in the logarithmic nature of the benthic boundary layer measured by the long-term lander ADCPs. Velocities at the East of Haig Fras lander site show distinct spring-neap tidal cycles, however there is little seasonal signal, which may be related to missing data over the peak winter months where waves would have a greater potential influence. The percentage of time the critical threshold is exceeded for a running 25 h window is also indicated, approximately showing daily resuspension events.

It should be noted that there is a lack of concurrent short- and long-term lander data for the other sites, which prevents this analysis being expanded for each of the processes sites. However, an assessment was made of the number of times over the measurement period that the critical threshold for erosion is exceeded based on calculated applied bed shear stresses from these landers, which is presented in Table 5 as exceedance percentages for periods where the ADCP velocity profiles were log-linear. These values indicate relative differences between the sites and the percentage exceedance ranges agree the values calculated for Benthic I and presented in Fig. 5.

These results corroborate those of the short-term lander deployments, that resuspension is most likely at Benthic A, and least common at Benthic G., but that resuspension is frequent in all regions of the Celtic Sea, occurring daily; and higher exceedance values in winter indicate a potential seasonal wave influence.

An analysis of wave data (Fig. 6) collected to the south west of the study sites, in the Central Celtic Sea (Triaxyal directional wave buoy) shows an increase in significant wave height (H_s) and period (T) during the winter months (October - March). Orbital velocities at the bed were calculated from the buoy data using a parametric method assuming a Donelan spectra (Wiberg and Sherwood, 2008; Donelan et al., 1985). Values of Tp and Hs were scaled by 10-year average values (Bricheno et al., 2015) to account for smaller waves and short peak periods at the benthic sites than at the wave buoy location. Maximum orbital velocities during December and March show agreement with the wave height. Despite the approximately 100 m depth, wave effects are felt at the bed. In general, wave orbital velocities during the August deployment were low, except at Benthic A, but when considering the yearlong data, there are several instances of orbital velocities exceeding 25–50 cm/s, and we would expect to see wave-induced resuspension during these times.

Table 5
Percentage of times where the critical erosion threshold is exceeded, based on the range of critical shear stresses measured over the entire study.

Month	*Benthic A*	*Benthic I*	*Benthic H*	*Benthic G*
April		55–89	48–84	35–65
May		59–93	51–89	37–66
June		53–90	44–86	24–54
July		66–94	58–91	
Aug		58–92	52–88	
Sept		64–95	57–91	
Oct		61–94	43–92	
Nov	80–99			
Dec	78–98			
Jan	65–98			
Feb	70–97			
March	67–97	61–95	56–90	
April	64–95	70–97	62–93	
May		72–97	63–92	
June		66–95	59–91	
July		74–98	68–97	
Aug		69–97	62–93	

Peaks in resuspension likelihood during the winter months are likely due to the influence of increased wave orbital velocities. This can be further confirmed by ADCP backscatter from the long-term landers (Fig. 7). Wavelet analysis of the near-bed ADCP backscatter indicates the temporal variability of the different mechanisms responsible for resuspension. To that end, the 5-min burst averaged acoustic signal strength has been converted to decibels following Deines (1999) to provide hourly values. A continuous wavelet transform is then applied to the ADCP backscatter, with a Morlet (k0 = 6) mother wavelet. Significant power is repeatedly found at diurnal periods (i.e. 24 h) at all sites. This is due to backscatter from zooplankton and diel migration, which was confirmed by matching the ADCP backscatter signal to sunrise and sun set times (not shown). The ADCP backscatter consistently displays spring-neap variability (large power value for periods around approximately 350 h) and there is also significant power at semi-diurnal periods. Both are clearly linked to tidal processes. The

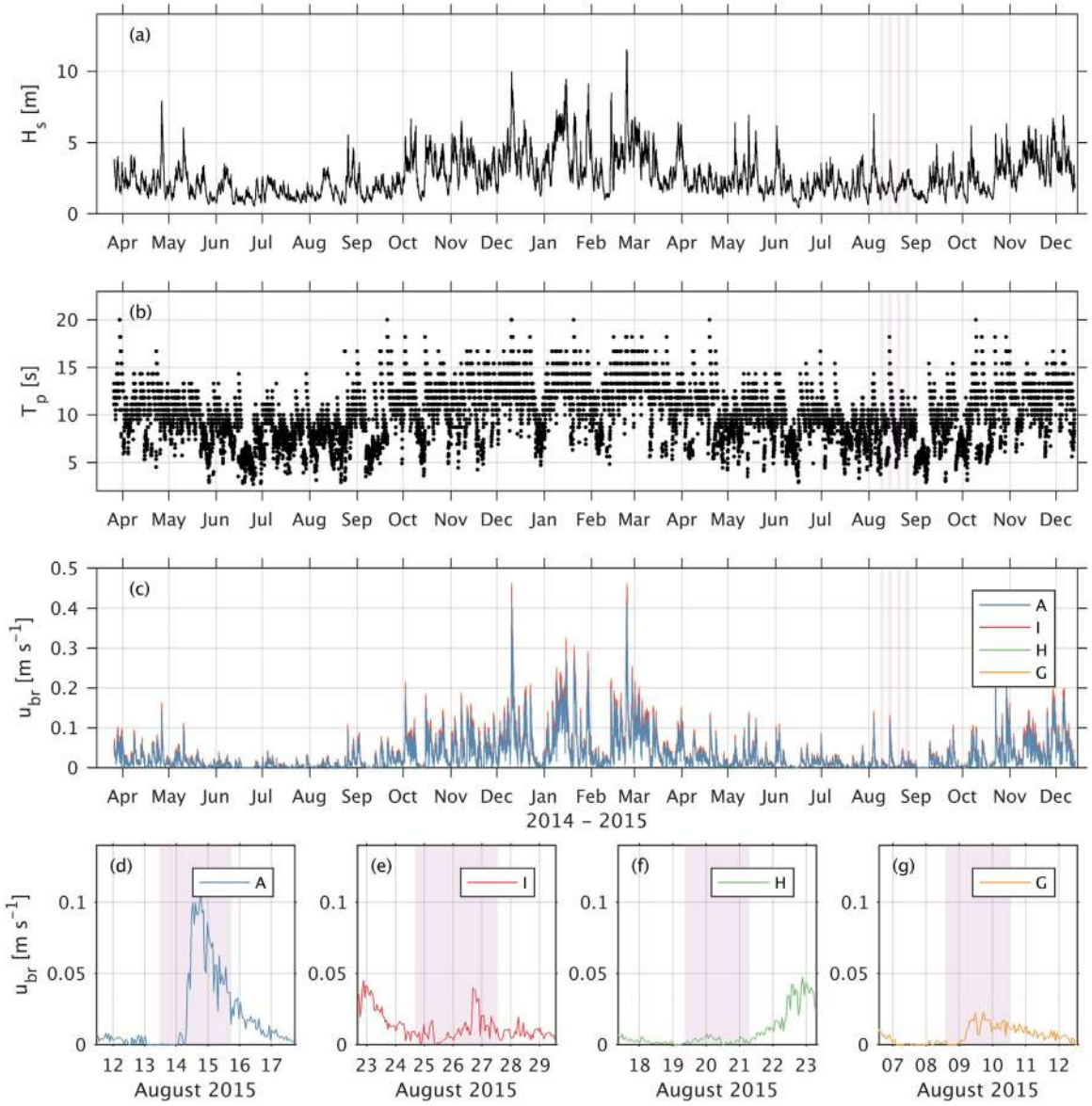

Fig. 6. Wave data from Triaxyal Directional wave Buoy located in the Central Celtic Sea (49.4N, 8.6W, grey). (a) Significant wave height. (b) Significant wave period. (c) Bed orbital velocities at the four benthic sites with timings of four miniSTABLE deployments indicated by lilac shading for August 2015. (d-g) Bed orbital velocities at each site during the August 2015 deployments (shaded in lilac).

semi-diurnal variability is indicative of advection of suspended particulate matter above non-resuspending beds (e.g., Weeks et al., 1993; Jago et al., 1993; Souza et al., 2007). This is more clearly marked at the sandier sites (Nymph Bank and Celtic Deep 2, Fig. 7 right panel) compared with East of Haig Fras (left panel). The spatial difference may be attributed to resuspension being easier at East of Haig Fras (which corresponds to Benthic H and I) compared with Nymph Bank/CD2L (corresponding to Benthic G), consistent with the noted spatial variability in critical erosion threshold (Section 3.2.1). Backscatter spring-neap variability is likely due to variability in tidal resuspension, as tidal advection would not be sufficient on its own (i.e. it would affect how far suspended sediments can travel but not how much is in suspension). Finally, there is also significant variability of the ADCP near-bed backscatter in the range 32–128 h, or approximately 1.3–5.3 days, which is likely due to storm resuspension. The peaks in wavelet transform power correspond to elevated values of the wave orbital velocity, even though not all orbital velocity peaks seem to lead to increased variability in ADCP backscatter. Even though we lack a complete time series at either long-term location, this “storm resuspension” variability in the ADCP backscatter does seem to have the expected seasonal variability, with more storm resuspension between October and April.

In general, the likelihood for the Celtic Sea appears higher than that seen in the North Sea experiments (Thompson et al., 2011), where critical erosion rates were higher, and high exceedance values only seen during the winter months when waves had a greater influence. It is possible that at the shallower North Sea sites, waves mobilise surface sediments during winter storms, which are then advected away by tidal currents. This removal of surface sediment, and erosion into the bed leaves remaining material that is more resistant to erosion However, in the deeper Celtic Sea, wave influences (although not absent) are lower, and reworking of the surface sediments is due to more chronic tidal processes. This may indicate that there are differences in the behaviour of shelf seas as opposed to more open shelf environments. There are also differences in sediment source in the two locations, with riverine inputs of SPM five times higher to the North Sea than the Celtic Sea (Ospar, 2016).

Further work will include using these findings to scale-up to the entire shelf-system, based on (1) using spatial measurements of bed

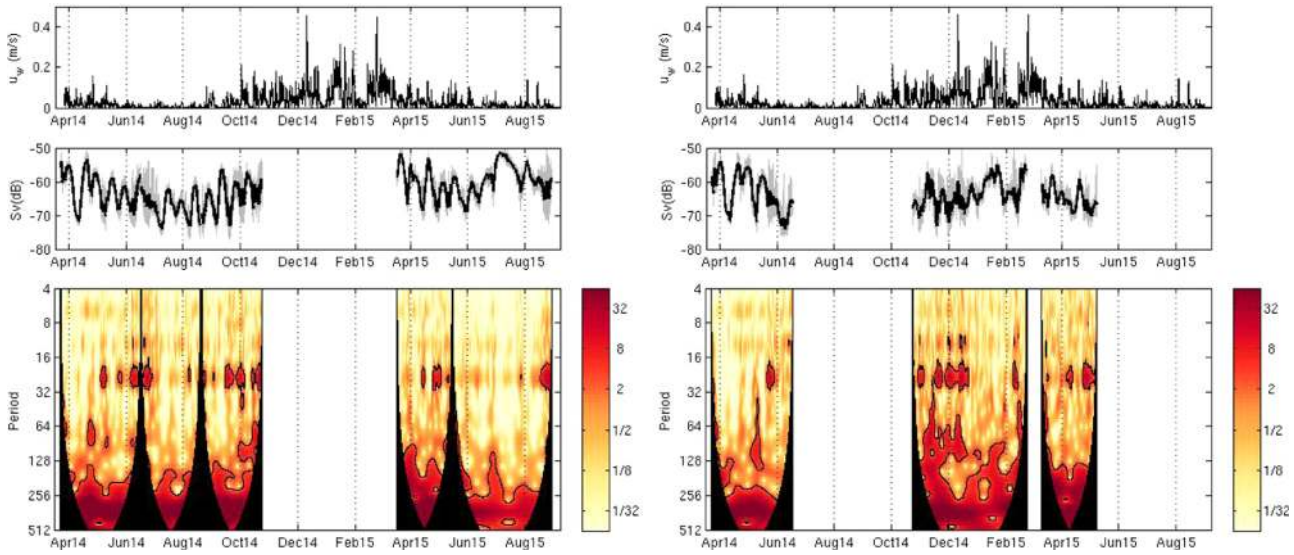

Fig. 7. Time frequency analysis of ADCP backscatter at the bottom ADCP bin (~ 3 m above bed) at the East of Haig Fras site (left) and the Nymph Bank (spring 2014) and Celtic Deep 2 (winter 14/15 and spring 2015) sites (right). Top: Bottom orbital velocity. Middle: Bottom bin ADCP backscatter measured hourly (grey) after application of a 30 h moving average (black line). Bottom panel: Time series of power of the continuous wavelet transform of ADCP backscatter in units of normalised variance. Solid black lines mark the 95% confidence intervals with respect to white noise and the black areas the cones of influence.

parameters to predict spatial variations in the critical erosion threshold, and (2) using models of applied bed shear stress over the shelf (currently in development) to assess likelihood of exceedance of these critical thresholds. This will then be used in conjunction with assessments of nutrient and carbon exchanges during resuspension events to assess the importance of resuspension at the shelf-scale.

5. Conclusions

Bed stability and critical erosion thresholds were determined for four sites in the Celtic Sea over a single annual seasonal cycle. These were used to assess predictors for erosion threshold in the region, and the likelihood and frequency of resuspension. Bulk density was found to be a reasonable predictor for erosion threshold ($R^2 = 0.73$), however a multi-parameter model based on a number of physical bed characteristics including grain size, sorting, kurtosis, bulk density, porosity, percentage fines, organic carbon content and chlorophyll *a* concentration was more accurate ($R^2 = 0.98$) and is recommended if the required data are available. A comparison of prevailing hydrodynamic conditions and critical erosion thresholds suggests frequent reworking and resuspension of the sediments at all sites, being greatest at the muddiest site Benthic A where resuspension occurs under > 60% of forcing scenarios. Resuspension is driven by tidal forcing year-round, but is enhanced by wave action during the winter months. This is confirmed by in situ measurements of backscatter. Comparisons with other UK shelf sea data from the North Sea shows significant differences in critical erosion thresholds, which may be related to differences in water column depths but also limited available data. It is clear that very localised variability in sediment characteristics, even considering a limited range of water column depths, makes prediction of erosion thresholds and therefore resuspension likelihood very difficult, and we suggest that given this and a lack of available benthic data, a generalised shelf sediment predictor is not currently possible, and that localised (shelf or region specific) predictors are still necessary.

Acknowledgements

This work was conducted under Work package 2 of the Shelf Sea Biogeochemistry programme (SSB WP2, NE/K001906/1; NE/K002015/1; NE/K001744/1; NE/K001914/1; NE/K00204X/1; NE/K001809/1; NE/K002139/1; NE/K001639/1; NE/K001922/1, 2011–2017), jointly funded by the Natural Environment Research Council (NERC) and the Department for Environment, Food and Rural Affairs (Defra). The views expressed are those of the author(s) and not necessarily those of NERC or Defra. We extend our thanks to the crew and scientists aboard the RSS Discovery cruises DY008, DY021, DY030 and DY034 and RV Cefas Endeavour cruises 22/14, 03/15 who provided the essential support needed for the collection of the data presented. Thanks go to Cefas and NOC for their support of the Lander and SmartBuoy deployments and maintenance. Thanks to Jo Hopkins from NOC and Jon Turton from the UK MetOffice for provision of the wave data. Thanks to Briony Silburn for the production of Fig. 1.

References

Ahmad, M.F., Dong, P., Mamat, M., Wan Nik, W.B., Mohd, M.H., 2011. The critical shear stress for sand mud mixtures. Appl. Math. Sci. 5, 53–71.
Amos, C.L., Gaborn, G.R., Christian, H.A., Atkinson, A., Robertson, A., 1992. In situ erosion measurements on fine-grained sediments from the Bay of Fundy. Mar. Geol. 108, 175–196.
Amos, C.L., Feeney, T., Sutherland, T.F., Luternauer, J.L., 1997. The stability of fine-grained sediments from the Fraser River Delta. Estuar. Coast. Shelf Sci. 45 (507e524).
Amos, C.L., Droppo, I.G., Gomex, E.A., Murphey, T.P., 2003. The stability of a remediated bed in Hamilton Harbour, Lake Ontario, Canada. Sedimentology 50, 149–168.
Amos, C.L., Umgiesser, G., Ferrarin, C., Thompson, C.E.L., Whitehouse, R.J.S., Sutherland, T.F., Bergamasco, A., 2010. The erosion rates of cohesive sediments in Venice lagoon, Italy. Cont. Shelf Res. 30 (859e870).
Andersen, T.J., 2001. Seasonal variation in erodibility of two temperate, microtidal mudflats. Estuar. Coast. Shelf Sci. 53 (1), 1–12.
Black, K.S., Tolhurst, T.J., Paterson, D.M., Hagerthey, S.E., 2002. Working with natural cohesive sediments. J. Hydraul. Eng. 128 (1) (2e8).
Bricheno, L.M., Wolf, J., Aldridge, J., 2015. Distribution of natural disturbance due to wave and tidal bed currents around the UK. Cont. Shelf Res. 109, 67–77. http://dx.doi.org/10.1016/j.csr.2015.09.013.
Burdige, D., 2006. Geochemistry of Marine Sediments. Princeton University Press, USA.
Couceiro, F., Fomes, G.R., Thompson, C.E.L., Statham, P.J., Sivyer, D.B., Parker, R., Kelly-Gerreyn, B.A., Amos, C.L., 2013. Impact of resuspension of cohesive sediment at the Oyster Grounds (North Sea) on nutrient exchange across the sediment-water interface. Biogeochemistry 113, 37–52. http://dx.doi.org/10.1007/s10533-012-9710-7.
Cross, J., Nimmo-Smith, W.A.M., Torres, R., Hosegood, P.J., 2013. Biological controls on resuspension and the relationship between particle size and the Kolmogorov length scale in a shallow coastal sea. Mar. Geol. 343, 29–38.
Davis, W.R., 1993. The role of bioturbation in sediment resuspension and its interaction with physical shearing. J. Exp. Mar. Biol. Ecol. 171 (2), 187–200.
De Souza, F.M., Filbert, E.R., de Camargo, M.G., Pieper, W.W., 2013. The spatial distribution of the subtidal benthic macrofauna and its relationship with environmental factors using geostatistical tools: a case study in Trapande Bay, southern Brazil. Zoologia 30 (1), 55–65.
Deines, K.L., 1999. Backscatter estimation using broadband acoustic Doppler current profilers, in: Proceedings of the IEEE/OES 6th Working Conference on Current

Measurement Technology, Inst. of Electr. and Electr. Eng., Piscataway, N. J., pp. 259–264.
Donelan, M.A., Hamilton, J., Hui, W.H., 1985. Directional spectra of wind-generated ocean waves. Philos. Trans. R. Soc. Lond. A 315 (1534), 509–562. http://dx.doi.org/10.1098/rsta.1985.0054.
Folk, R.L., 1954. The distinction between grain size and mineral composition in sedimentary rocks. J. Geol. 62, 344–359.
Folk, R.L., Ward, W.C., 1957. Brazos River bar: a study in the significance of grain size parameters. J. Sediment. Petrol. 27, 3–26.
Germano, J.D., Rhoads, D.C., Valente, R.M., Carey, D.A., Solan, M., 2011. The use of sediment profile imaging (API) for environmental impact assessments and monitoring studies: lessons learned from the past four decades. Oceanogr. Mar. Biol.: Annu. Rev. 49, 235–298.
Grabowski, R.C., Droppo, I.G., Wharton, G., 2011. Erodibility of cohesive sediment: the importance of sediment properties. Earth Sci. Rev. 105 (3–4), 101–120.
Harris, P.T., 2014. Shelf and deep sea sedimentary environmentsl and physical benthic disturbance regimes: a review and synthesis. Mar. Geol. 353, 169–184.
Hong, A., Tao, M., Kudrolli, A., 2015. Onset of erosion of a granular bed in a channel driven by fluid flow. Phys. Fluids 27, 013301.
Houwing, E.J., 2000. Sediment Dynamics in the Pioneer Zone in the Land Reclamation Area of the Wadden Sea, Graningen The Netherlands, Ph.D. Thesis.
Hydrographic Office, 1996. Co-tidal and Co-range lines: British Isles and Adjacent waters (Admiralty Chart No. 5058). UK Hydrographic Office, Taunton, UK.
Jacobs, W., Le Hir, P., Van Kesteren, W., Cann, P., 2011. Erosion threshold of sand-mud mixtures. Cont. Shelf Res. 31 (10), S14–S25.
Jago, C.F., Bale, A.J., et al., 1993. Resuspension processes and seston dynamics, southern North Sea. Philos. Trans. R. Soc. Lond. A343, 475–491.
Jennings, S., Lee, J., Hiddink, J.G., 2012. Assessing fishery footprints and trade-offs between landings value, habitat sensitivity, and fishing impacts to inform marine spatial planning and an ecosystem approach. ICES J. Mar. Sci. 69 (6), 1053–1063.
Joint, I., Owens, N., Pomroy, A., Pomeroy, A., 1986. Seasonal production of photosynthetic picoplankton and nanoplankton in the Celtic Sea. Mar. Ecol. Progress. Ser. 28 (3), 251–258.
Katz, T., Yahel, G., Tunnicliffe, V., Herut, B., Whitney, F., Snelgrove, P.V.R., Lazar, B., 2016. The silica cycle in a Northeast Pacific fjord; the role of biological resuspension. Progress. Oceanogr. 147, 10–21.
Komar, P.D., 1987. Selective grain entrainment by a current from a bed of mixed sizes; a reanalysis. J. Sediment. Res. 57, 203–211.
Li, M.Z., Gust, G., 2000. Boundary layer dynamics and drag reduction in flows of high cohesive sediment suspensions. Sedimentology 47, 71–86.
Low, B.A., Hill, P./S./ Milligan, Curran, T.G., WIberg, K.J., L, P., Wheatcroft, R.A., 2008. Size sorting of fine grained sediments during erosion: results from the western Guld of Lias. Cont. Shelf Res. 28, 1935–1946.
Marsay, C.M., Sedwick, P.N., Dinniman, M.S., Barrett, P.M., Mack, S.L., McGillicuddy Jr, D.J., 2014. Estimating the benthic efflux of dissolved iron on the Ross Sea continental shelf. Geophys. Res. Lett. 41 (21), 7576–7583.
Masselink, G. Scott, T. Poate, T. Russell, P. Davidson, M., Conley, D., 2015. The Extreme 2013/2014 Winter Storms: Hydrodynamic Forcing and Coastal Response along the Southwest Coast of England.
Mitchener, H., Torfs, H., 1996. Erosion of mud/sand mixtures. J. Coast. Eng. 29, 1–25.
Morris, A.W., Howarth, M.J., 1998. Bed stress induced sediment resuspension (SERE 88/89). Cont. Shelf Res. 18 (11), 1203–1213.
Morris, J.T., Barber, D.C., Callaway, J.C., Chambers, R., Hagen, S.C., Hopkinson, C.S., Johnson, B.J., Megonigal, P., Neubauer, S.C., Troxler, T., Wigand, C., 2016. Contributions of organic and inorganic matter to sediment volume and accretion in tidal wetlands at steady state. Earths Future 4, 110–121.
Nittrouer, C.A., Wright, L.D., 1994. Transport of particles across continental shelves. Rev. Geophys. 32 (1), 85–113.
Ospar, 2016. Riverine Inputs and Direct Discharges to Convention Waters OSPAR Contracting Parties' RID 201 4 Data Report. p. 83.
Paphitis, D., 2001. Sediment movement under unidirectional flows: an assessment of empirical threshold curves. Coast. Eng. 43, 227–245.
Parker, R.E., 1999. The Role of Colloidal Material in the Fate and Cycling of Trace Metals and Estuarine and Coastal Waters (Ph.D. Thesis). University of Southampton, UK.
Pye, K., Tsoar, H., 2009. Aeolian Sand and Sand Dunes. Springer, Germany.
Queste, B.Y., Fernand, L., Jickells, T.D., Heywood, K.J., Hind, A.J., 2016. Drivers of summer oxygen depletion in the central North Sea. Biogeosciences 13, 1209–1222.
Rhoads, D.C., Cande, S., 1971. Sediment profile camera for in situ study of organism-sediment relations. Limnol. Oceanogr. 16 (1), 110–114. http://dx.doi.org/10.4319/lo.1971.16.1.0110.
Santisteban, J.I., Mediavilla, R., Lopez-Pamo, E., Dabrio, C.J., Ruiz Zapata, M.B., Garcia, M.J.G., Castano, S., Martinex-Alfaro, P.E., 2004. Loss on ignition: a qualitative or quantitative method or organic matter and carbonate mineral content in sediments? J. Paleolimnol. 32 (3), 287–299.
Schallenberg, M., Burns, C.W., 2004. Effects of sediment resuspension on phytoplankton production: teasing apart the influences of light, nutrients and algal entrainment. Freshw. Biol. 49, 143–159. http://dx.doi.org/10.1046/j.1365-2426.2003.01172.x.
Shi, B., Wang, Y.P., Yang, Y., Li, M., Li, P., Ni, W., Gao, J., 2015. J. Coast. Res. 31 (6), 1344–1356.
Simpson, J.H., Sharples, J., 2012. Introduction to the Physical and Biological Oceanography of Shelf Seas. Cambridge University Press, UK.
Solan, M., Godbold, J., Thompson, C., Ruhl, H., Mayor, D., Crippts, G., 2017. Biogeochemistry, macronutrient and carbon cycling in the benthic layer. Nerc. Impact 7, 11–15.
Soulsby, R.L., 1983. The bottom boundary layer of shelf seas. In: Johns, B. (Ed.), Physical Oceanography of Coastal and Shelf Seas. Elsevier, Amsterdam, pp. 189–266 (Souza).
Souza, A.J., Holt, J.T., Proctor, R., 2007. Modelling SPM on the NW European shelf seas. Geological Society 274. Special Publications, London, pp. 147–158.
Staudt, F., Mullarney, J.C., Pilditch, C.A., Huhn, K., 2017. The role of grain-size ratios in the mobility of mixed granular beds. Geomorphology 278, 314–328.
Su, J., Tian, T., Krasemann, H., Schartau, M., Wirtz, K., 2015. Response patterns of phytoplankton growth to variations in resuspension in the German Bight revealed by daily MERIS data in 2003 and 2004. Oceanologia 57 (4), 328–341.
Sutherland, T.F., Amos, C.L., Grant, J., 1998. The erosion threshold of biotic sediments: a comparison of methods. In: Sedimentary Processes in the Intertidal Zone 139 Geological Society of London, Special Publications, UK.
Tett, P.B., Walne, A., 1995. Observations and simulations of hydrography, nutrients and plankton in the southern North Sea. Ophelia 42, 371–416.
Thompson, C.E.L., Couceiro, F., Fones, G.R., Helsby, R., Amos, C.L., Black, K., Parker, E.R., Greenwood, N., Statham, P.J., Kelly-Gerreyn, B.A., 2011. In situ flume measurements of resuspension in the North Sea. Estuar. Coast. Shelf Sci. 94, 77–88.
Thompson, C.E.L., Coucerio, F., Fones, G.R., Amos, C.L., 2013. Shipboard measurements of sediment stability using a small annular flume - core Mini Flume (CMF). Limnol. Oceanogr.: Methods 11, 604–615.
Thompson, C.E.L., Silburn, B., Williams, M.E., Hull, T., Sivyer, D., Amoudry, L.O., Widdicombe, S., Ingels, J., Carnovale, G., McNeill, C.L., Hale, R., Laguionie Marchais, C., Hicks, N., Smith, H., Klar, J.K., Hiddink, J.G., Kowalik, J., Kitidis, V., Reynolds, S., Woodward, E.M.S., Tate, K., Homoky, W.B., Kröger, S., Godbold, J.A., Aldridge, J., Mayor, D.J., Benoist, N.M.A., Bett, B.J., Morris, K.J., Parker, E.R., Ruhl, H., Statham, P.J., Solan, M., 2017. An approach for the identification of exemplar sites for scaling up targeted field observations of benthic biogeochemistry in heterogeneous environments. Biogeochemistry 135 (1–2), 1–34.
Thomsen, L., Gust, G., 2000. Sediment erosion thresholds and characteristics of resuspended aggregates on the western European continental margin. Deep Sea Res. Part 1: Oceanogr. Res. Pap. 47 (10), 1881–1897.
Thomsen, L., McCave, I.N., 2000. Aggregation processes in the benthic boundary layer at the Celtic Sea continental margin. Deep Sea Res. Part 1: Oceanogr. Res. Pap. 47 (8), 1389–1404.
Uncles, R.J., Stephens, J.A., 2007. Sea 8 Technical Report - Hydrography. Strategic Environmental Assessment Programme. UK Dept. of Trade and Industry, UK, pp. 105.
Underwood, G.J.C., Paterson, D.M., 1993. Seasonal changes in diatom biomass, sediment stability and biogenic stabilisation in the severn estuary. J. Mar. Biol. Assoc. UK 73, 871–887.
Van Ledden, M., 2003. Sand and Mud Segregation (Ph.D. Thesis). Delft University of Technology, Netherlands.
Wainright, S.C., Hopkinson, C.S., 1997. Effects of sediment resuspension on organic matter processing in coastal environments: a simulation model. J. Mar. Syst. 11, 353–368.
Weeks, A.R., Simpson, J.H., Bowers, D., 1993. The relationship between concentrations of suspended particulate material and tidal processes in the Irish Sea. Cont. Shelf Res. 13 (12), 1325–1334.
Wiberg, P.L., Sherwood, C.R., 2008. Calculating wave-generated bottom orbital velocities from surface-wave parameters. Comput. Geosci. 34 (10), 1243–1262. http://dx.doi.org/10.1016/j.cageo.2008.02.010.
Widdows, J., Brinsley, M.D., Salkeld, P.N., Lucas, C.H., 2000. Influence of biota on spatial and temporal variation in sediment erodability and material flux on a tidal flat (Westerschelde, The Netherlands). Mar. Ecol. Progress. Ser. 194 (23e37).
Widdows, J., Friend, P.L., Bale, A.J., Brinsley, M.D., Pope, N.D., Thompson, C.E.L., 2007. Inter- comparison between five devices for determining erodability of intertidal sediments. Cont. Shelf Res. 27.
Young, R.N., SOuthard, J.B., 1978. Erosion of fine-grained marine sediments: sea floor and laboratory experiments. Geol. Soc. Am. Bull. 89, 663–672.